Article, Published Version

Brinkgreve, Ronald B. J.; Bürg, Markus; Andreykiv, A.; Lim, Liang J.

Beyond the Finite Element Method in Geotechnical Analysis

BAWMitteilungen

Beyond the Finite Element Method in Geotechnical Analysis

Über die Finite-Elemente-Methode in der geotechnischen Analyse hinaus

Dr. Ronald B. J. Brinkgreve, Delft University of Technology & Plaxis BV
Dr. Markus Bürg, Dr. Andriy Andreykiv, Mr. Liang Jin Lim, Plaxis BV, Delft

The finite element method (FEM) has obtained a strong position in geotechnical analysis and design, next to conventional design methods. However, FEM is more suited for situations involving complex geometries and soil-structure interaction. Nevertheless, FEM also has its limitations, in particular when it comes to large deformations and material flow, as it occurs when installing offshore foundations and pipelines in the seabed. In such cases the recently developed material point method (MPM) is much more suitable to deal with the effects of large deformations.

This contribution gives an introduction to MPM for geotechnical analysis. In addition, it demonstrates its use for geotechnical offshore applications (for example the installation of piles and anchors in the seabed, spudcan penetration and extraction, the creation of trenches for pipelines and cables, and the movement of pipelines in the seabed). This contribution presents some of the challenges when using MPM in practical applications, since MPM calculations are more time consuming and more sensitive to inaccuracies than FEM calculations. Topics that are discussed are the use of DDMP (dual-domain material point method) to enhance the 'smoothness' of the solution and to improve the accuracy of stresses in the case of material points moving from one cell to another, how to deal with 'empty' cells, determination of active domain boundaries, connecting MPM to FEM and the application of loads and boundary conditions. The presented solutions are meant to facilitate the use of MPM on a larger scale for geotechnical engineering applications.

Die Finite-Elemente-Methode (FEM) ist inzwischen auch in der geotechnischen Analyse ein häufig benutztes Werkzeug. Insbesondere ist FEM sehr gut für Anwendungen mit komplexen Geometrien und Boden-Bauwerk-Interaktionen geeignet. Nichtsdestotrotz hat FEM natürlich auch seine Einschränkungen. Dies ist insbesondere der Fall, wenn es zu großen Verformungen und Materialflüssen, wie z. B. in der Installation von Offshore-Fundamenten oder Pipelines im Meeresboden üblich, kommt. Für solche Anwendungen ist die Material-Punkt-Methode (MPM) eine deutlich bessere Alternative, um das Auftreten von großen Verformungen zu simulieren.

Dieser Beitrag soll eine Einführung in MPM anhand einer geotechnischen Analyse geben. Die praktische Anwendbarkeit wird anhand von verschiedenen geotechnischen Offshore-Anwendungen (z. B. Installation von Pfählen und Ankern im Meeresgrund, Ziehen von Schutzgräben für Pipelines und Kabeln und Bewegung von Pipelines im Meeresgrund) demonstriert. Dabei wird auch auf die unterschiedlichen Schwierigkeiten, die bei der Nutzung von MPM auftreten können, detaillierter eingegangen. Insbesondere soll diese Präsentation auch zu einer breiteren Verwendung von MPM in der geotechnischen Analyse anregen und die damit verbundenen Vorteile aufzeigen.

1 Introduction
Einleitung

The conventional finite element method (FEM) has been used for several decades to predict deformation of soil in geotechnical engineering. Certain geotechnical processes involve large displacements in the soil. Thus, conventional FEM cannot be used to analyse these types of problems because of the issue with mesh tan-

gling when the deformations of the mesh become extremely large. In recent years, a few alternatives to FEM have been introduced to simulate large deformation problems, particularly the material point method (MPM). MPM was first introduced by Sulsky et al. (1994) and has meanwhile been used in various geotechnical applications such as modelling of landslides, cone penetration (Beuth et al. 2011), pile penetration (Lim et al. 2013), and spudcan penetration (Lim et al. 2014). However, these applications are still performed from a research perspective rather than for engineering and design. MPM calculations are more time consuming and more sensitive for inaccuracies and numerical instability than FEM calculations. Hence, the use of MPM in practical applications brings some challenges. The following challenges and solutions are discussed in this contribution:

Expensive computational cost: By using a mesh relaxation method to connect the MPM analysis with FEM (see Lim et al. (2013) for further details), we have been able to limit the MPM computation to the area where potential large deformation will occur and can use conventional FEM in the other areas of the computational domain.

Contact algorithm: The MPM formulation already includes inherent rigid contact, but produces unrealistically rigid contact when used in soil-structure interaction problems. We have adopted a level-set large sliding contact algorithm introduced by Andreykiv et al. (2011). It uses two non-matching meshes to model the contact between the soil and the structure, such as in spudcan and pile penetration.

Volumetric locking: We have also introduced a mixed displacement-pressure (p-u) formulation (Brezzi et al., 1991) of FEM into our MPM implementation to resolve the volumetric locking of linear elements in undrained behaviour (incompressibility) by decoupling the volumetric stress and the deviatoric stress terms from the total stress.

Critical time step: The explicit formulation of MPM has a severe limitation of the maximal time step size to avoid instability issues. Therefore, we have chosen an implicit formulation of MPM to eliminate this time stepping issue and be able to select also larger time steps. Furthermore, the existing FEM technologies formulated in implicit schemes can be directly integrated into MPM calculations.

This paper is structured as follows: In Chapter 2 provides an introduction to MPM and its implicit formulation. The major challenges and its corresponding solutions are discussed in Chapter 3. Chapter 4 presents some applications of the method in offshore geotechnical engineering. The last chapter draws some conclusions on the use of MPM in practical applications.

2 Implicit formulation of MPM
Implizite Formulierung der MPM

First, let us give an introduction to MPM, which has similarities with FEM, for geotechnical analysis. MPM can be regarded as FEM where the integration points (material points) are moving through the grid. A MPM calculation step can be divided into three phases: The initialisation phase, the Lagrangian phase and the convection phase (Fig. 1).

Phases 1 and 2 are similar to FEM; the difference is in Phase 3. Since information of stress and material state is contained in the material points, which can move

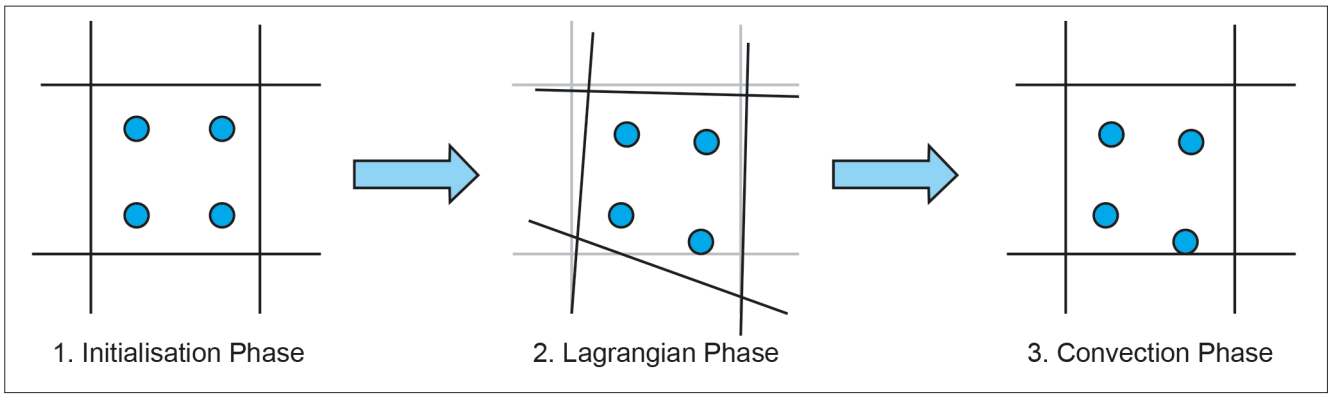

Figure 1: Three phases in an MPM calculation step
Bild 1: Die drei Phasen eines Berechnungsschritts bei der MPM

through the grid, it makes the method suitable for very large deformations.

Governing continuum equations

For a continuous body $\Omega \subset R^n$, n ∈ {2,3}, with a boundary $\Gamma = \partial w$, the conservation equations for mass and linear momentum governing the continuous body can be defined as

$$\frac{d\rho}{dt} + \rho \nabla \cdot v = 0 \tag{1}$$

$$\rho a = \nabla \cdot \sigma + \rho b \tag{2}$$

where ρ is the mass density, v is the velocity, a is the acceleration, σ is the Cauchy stress tensor, and b is the specific body force.

Discretization of continuum equations

To solve the continuum equations, the strong form of the equations is transformed into a weak form and discretized by using standard FEM procedures. After the multiplication with finite element shape functions, the linear momentum equation (2) becomes

$$\sum_{j=1}^{N} \boldsymbol{a}_j \int_{\Omega_c} \rho N_i N_j d\Omega_c = - \int_{\Omega_c} \nabla N_i : \sigma d\Omega_c + \int_{\Omega_c} \rho b N_i \, d\Omega_c + \int_{\Gamma_c} t N_i \, d\Gamma_c \tag{3}$$

Where N is the total number of degrees of freedom (DoF) in a computational domain c, i, j are its indices, $\boldsymbol{a}_j$ is the acceleration at DoF j, N_i is the shape function of DoF i, $\mathbf{t}$ is the surface traction, and Γ_c is the surface boundary of the computation domain Ω_c . The first term of the right hand side of (3) is defined as the internal force of the system, $\mathbf{f}_{int}$. The sum of the second and the third terms of the right hand side can also be defined as the external force of the system, $\mathbf{f}_{ext}$. Meanwhile, comparable to conventional FEM, the numerical integration of MPM over Ω_c is approximated by summing the weight contribution of each material point as follows

$$\int_{\Omega_e} F \, d\Omega_e \approx \sum_{p=1}^{N_p} v_p F(\mathbf{x}_p) \tag{4}$$

F is an arbitrary function to be integrated over the element, $\mathbf{x}_p$ is the location of material point p and v_p is the volume of the material point p. The internal force vector $\mathbf{f}_{int}$ can then be approximated by

$$\mathbf{f}_i^{int} = \int_{\Omega_c} \nabla \mathbf{N}_i : \sigma \, d\Omega \approx \sum_{p=1}^{N_p} v_p \nabla \mathbf{N}_i : \sigma_p(\mathbf{x}_p) \tag{5}$$

Implicit time integration scheme

Solving a single step in MPM is identical to conventional FEM. The Newton-Raphson method is adopted to solve the equation of motion implicitly. The linearized equation of motion during a Newton iteration k for an arbitrary time step is defined as (Wieckowski 2004)

$$\mathbf{K}_{ij}^{k-1} \cdot d\mathbf{u}_j = (\mathbf{f}_i^{ext}) - (\mathbf{f}_i^{int})^{k-1} - \mathbf{m}_{ij} \cdot \boldsymbol{a}_j^{k-1} := \mathbf{Q}_j^k \tag{6}$$

where $\mathbf{K}$ is the tangent matrix of the system, $\mathbf{m}$ is the mass matrix, $d\mathbf{u}_j$ is the incremental displacement of DoF j, $\mathbf{Q}$ is the residual vector, and k is the iteration step. Equation (6) is solved iteratively, until the residual of the system is less than a defined convergence criteria $\mathbf{Q} < \varepsilon$. The displacement update is given as

$$\mathbf{u}_j^k = \mathbf{u}_j^{k-1} + d\mathbf{u}_j \tag{7}$$

The acceleration term can be calculated by discretizing the time derivative with a trapezoidal rule. The discretized acceleration term is given as

$$\mathbf{a}_j^k - \frac{4}{\Delta t^2} \mathbf{u}_j^{k-1} - \frac{4}{\Delta t} \mathbf{v}_j^0 - \boldsymbol{a}_j^0 \tag{8}$$

where the $\mathbf{v}_j^0$ and $\mathbf{a}_j^0$ terms are the nodal velocity and acceleration at the start of the time step.

Numerical implementation of implicit dynamic MPM

At the beginning of a calculation step, all state variables are stored in the material points. These state variables are then interpolated to the computational grid using the standard shape function interpolation. The nodal velocity (and nodal acceleration) can be interpolated by using conservation of momentum

$$m_i \mathbf{v}_i = \sum_{p=1}^{N_p} \rho \upsilon_p \mathbf{N}_i(\mathbf{x}_p) \mathbf{v}_p \tag{9}$$

As the computational grid represents the current configuration of the model, the Updated Lagrangian formulation of discrete equations is used. In this formulation, the elasticity tangent matrix is defined by

$$\mathbf{K}_{ij}^{k-1} = \int_{\Omega_c} \nabla \mathbf{N}_i : \mathbf{C}^{\sigma\tau} : \nabla \mathbf{N}_j \, d\Omega_c + \int_{\Omega_c} \nabla \mathbf{N}_i : \mathbf{I}\sigma : \nabla \mathbf{N}_j \, d\Omega_c \tag{10}$$

$\mathbf{C}^{\sigma t}$ is the fourth order tensor of Truesdell rate of elastic tangent modulus and $\boldsymbol{\sigma}$ is the Cauchy stress tensor. Equation (10) also shows that the tangent matrix includes terms of material nonlinearity (first term) and geometrical nonlinearity (second term). The tangent modulus tensor depends on the constitutive model of the material and will not be elaborated here. Equation (10) is solved to obtain the incremental displacement $d\mathbf{u}$. The computational grid is then deformed with the solution, and the kinematics of the system is then updated before the next iteration begins. The update of the velocity term is given by

$$\mathbf{v}_i^k = \mathbf{v}_i^{k-1} + \frac{2}{\Delta t} d\mathbf{u}_i^k - \mathbf{v}_i^0 \tag{11}$$

while the nodal acceleration is updated by using (8).

After the Newton procedure has satisfied the required-convergence criteria, a convective stage is carried out in the MPM region to update the state variables from the computational grid back to the material points. The convection step is performed by interpolating nodal results from the computational grid to the material points with standard approximation functions defined on the mesh. Once the convective stage has been carried out, the deformed computational grid can be discarded because all the state information is now stored in the material points. As a result, excessive mesh distortion is prevented.

3 Challenges of MPM calculations
Herausforderungen von MPM-Berechnungen

MPM calculations are more time consuming and more sensitive to inaccuracies than FEM calculations. Hence, the use of MPM in practical applications brings some challenges. In this section, we will discuss a number challenges and its corresponding solutions.

3.1 Points moving from one cell to another
Punkte, die von einer Zelle in eine andere Zelle wandern

When a material point crosses the boundary of a cell, a discontinuity occurs in the gradient of the computed displacement which, for example, leads to inaccurate stresses. Without a proper treatment of this numerical noise, the application of MPM to cases with large deformations is severely limited, since the inaccurate stresses may cause a premature prediction of material failure and change the physical characteristics of the material. These inaccuracies can be reduced significantly by using an enhanced version of MPM, such as the generalised interpolation material point (GIMP) method (Bardenhagen & Kober 2004) or the dual domain material point (DDMP) method (Zhang et al. 2011). The latter will be discussed in more detail in 3.6.

The GIMP method is a family of extended MPMs, where material points are defined by so-called particle characteristic functions. These functions represent the space occupied by the respective particle and follow the same deformation as the discretised physical domain. In particular, the integration over the support of these functions poses a practical challenge. Whereas, in the one-dimensional case, the integration can still be performed analytically, as shown in (Bardenhagen & Kober 2004), one usually has to employ an expensive numerical integration technique for the two- and three-dimensional case. If the particle characteristic functions are chosen to be Dirac delta functions, the classical MPM from Sulsky et al. (1994) and Sulsky et al. (1995) is recovered.

In contrast to the GIMP method, the DDMP method does not require tracking the actual deformation of the particles. Instead of modifying the shape functions, it introduces a modified gradient definition which is continuous across cell boundaries. The support of this modified gradient is larger than the support of the shape function itself, but it is still limited to the cell in which the material point is located and its direct neighbours. Thus, the interaction between different material points is restricted to a quasi-local domain. In particular, the calculation of the modified gradient only requires an additional integration of the shape function and, thus, can be realised very easily. A more detailed discussion of the DDMP method will be provided in 3.6.

3.2 Dealing with empty cells
Umgang mit leeren Zellen

When all material points have left a cell, the cell has no stiffness or mass contributions in the global matrix. To avoid singularity of the system of equations, a small

elastic stiffness is placed in these empty cells. This procedure is also applied to 'buffer' cells (for example above the soil surface) that are initially empty, but are present to catch material points that are moving above the initial surface.

3.3 Determining active boundaries
Bestimmung aktiver Ränder

Since the active domain is formed by the (moving) material points rather than by the calculation grid itself, a special procedure is needed to determine the boundaries of the active domain occupied by the soil. For this purpose, we have developed a level-set formulation, where the actual boundary is given by the zero level-set. Then, this zero level-set isosurface can be used for integrating over the active boundary and, therefore, applying, e.g., boundary conditions on it (see also 3.5). In general, this approach allows for treatment of the boundaries as if their explicit formulation was available. Thus, no entirely new procedures for applying boundary conditions or determining computed quantities on the boundary have to be derived.

3.4 Connecting MPM to FEM domain
Verbinden von MPM- und FEM-Gebiet

Since MPM is 'expensive', it should be used only where really necessary, whereas parts of the domain that undergo relatively small deformations can be modelled by conventional FEM using an Updated Lagrangian formulation. This means that the FEM domain as well as the MPM domain can deform. Hence, the Convection Phase (Fig. 1.3) involves an elastic stretch (adhering to the deformations of the FEM mesh), rather than a full restoration of the original grid.

In the FEM domain, conventional quadrature points are used for computing the integrals, while the MPM domain uses material points as quadrature points. Because we are using an implicit formulation of MPM, the coupling between the FEM and MPM can be done naturally. The analysis procedure remains the same, except that, at the end of each calculation step, a mesh relaxation procedure is performed in the MPM domain to restore the deformed mesh in addition to the convection step of MPM. An artificial constraint is added to the FEM domain to prevent the mesh in the FEM domain from restoring, while the mesh in the MPM domain is relaxed back to its least deformed state by removing external loads contributing to the system. In this way, the mesh distortion problem in the MPM domain can be mitigated, while maintaining the validity of the deformation state of the FEM domain.

3.5 Application of loads and boundary conditions
Anwendung von Belastungen und Randbedingungen

Since model boundaries are determined by material points rather than by the domain boundaries, the application of loads and boundary conditions has to involve some special procedures. For basic boundary conditions, such as prescribed displacements and distributed loads, we can employ the level-set formulation described in 3.3 to calculate the corresponding boundary integrals.

However, due to possibly large deformations of the soil and, thus, also its boundaries, it has to be evaluated thoroughly whether a classical boundary condition acting always in the prescribed direction relative to the boundary is the correct choice. Often, the displacements and loads, which shall be applied, have the characteristics of a soil-body contact-interaction rather than a pure Dirichlet or Neumann boundary condition. This desired behaviour can be achieved by employing a full contact formulation as described in 3.7. In this way, it is guaranteed that the interaction between the freely moving soil and the physical body placed on top of it is resolved correctly.

3.6 Use of DDMP to 'smoothen' the solution
Anwendung von DDMP zur Glättung der Lösung

Discontinuities of stresses across cell boundaries as mentioned under 3.1 may be overcome by introducing a kind of C^1-continuity across cell boundaries. The DDMP method is a way to enforce such a 'smooth' transition across all cell boundaries in the calculation grid and, thereby, improving the accuracy of stresses. For a detailed introduction to the DDMP method, we refer to the original work by Zhang et al. (2011).

In addition to the DDMP method described in Zhang et al. (2011), we have extended its formulation by introducing a tangent stiffness for the DDMP formulation. The reason for this modification is that the original method was derived in an explicit scheme and, thus, is not suitable for our implicit MPM implementation. In general, DDMP results show less pollution of gradient quantities, such as stresses and strains, caused by numerical noise. As a side effect, DDMP also improves convergence of the Newton-Raphson method slightly compared to standard MPM.

3.7 Contact formulation
Formulierung von Kontakten

The algorithm for contact interaction between a spudcan, modelled with FEM and MPM based soil was initially introduced in Andreykiv et al. (2011). It is based on the minimization of the energy functional with a Lagrange multiplier and formulated as in classical contact mechanics. However, instead of employing a distance function between two contacting bodies, we use the above mentioned density-based level-set function which marks the boundary of the material points. Due to the fact that the level-set function is defined on the full soil domain, the spudcan surface is embedded into the soil domain and the contact constraint is enforced similar to the fictitious domain method (Glowinski et al., 1994).

3.8 Stability of calculation
Stabilität der Berechnung

Due to several additional tools and parameters available in MPM, e.g., number of material points per cell, size and stiffness of empty layer, treatment of boundary conditions, etc., it is very challenging to make MPM calculations as stable and as easy to use as it is known and expected from conventional FEM calculations. The large variety of possible combinations of all these parameters requires a significant effort to come up with a suitable choice working for all possible applications and, thus, not to require too much input from the end-user.

Apart from the successful selection of parameters, the conditioning of system matrices is generally worse in MPM than in FEM. Therefore, an efficient preconditioner, such as domain decompositioning and algebraic or geometric multigrid, is needed to be able to apply an iterative solver to the resulting linear systems of equations.

Often the convergence of a static MPM calculation can be improved, by reformulating it as a dynamic MPM calculation reaching a steady state. In the case of a dynamic calculation, the step size of the time discretisation has to be chosen carefully. Due to the additional phases required in each MPM step (see Figure 1), small step sizes are more expensive than in standard FEM calculations. However, due to the large deformations typically occurring in MPM calculations, the step size cannot be too large in order to be still able to solve the discrete nonlinear problem in each time step. Therefore, an adaptive time stepping scheme allowing for the automatic increment and decrement of the time step size whenever required is inevitable. In our calculations, the use of an adaptive Newmark-beta method with b = 0.5 instead of the standard undamped choice b = 0.25 proved to be a reasonable time stepping scheme.

4 Applications in offshore geotechnics
Anwendungen in der Offshore-Geotechnik

Very large deformations and material flow can occur, for example, in geotechnical offshore applications, such as the installation of piles and anchors in the seabed, spudcan penetration and extraction, the creation of trenches, as well as pipeline and cable movements. MPM is particularly useful for such applications (Lim et al. 2014).

The presented solutions as described in the previous chapter are meant to facilitate the use of MPM on a larger scale by geotechnical engineers in offshore engineering and other fields of applications. The remainder of this section describes some applications in which MPM has been used successfully.

4.1 Pile installation
Einbau von Pfählen

A first application involves the penetration of a sheet pile into the soil (after Lim et al. 2013), for which a 2D plane strain model is used (Fig. 2). Here, a fictitious

weightless soil is considered, modelled by means of the linear elastic perfectly plastic Tresca model with stiffness properties E_s = 100 kN/m² and n = 0.33, and different cohesive strengths of c = 0.25, 0.50 and 1.0 kN/m², respectively. The weightless sheet pile is modelled as a linear elastic volume with stiffness properties E_p = 20000 kN/m² and ν = 0.0.

The soil domain is divided into an MPM region, where large deformations and pile-soil contact are expected, and a FEM region further away from the pile, where smaller deformations occur. An MPM buffer region is used to catch material points moving above the ground surface. The analysis is performed using linear triangular elements as well as quadrilateral elements with a refinement around the pile. The pile-soil contact is not explicitly modelled and is obtained from the 'standard' MPM formulation. Each MPM element initially contains 12 material points for the triangular elements and 16 material points for the quadrilateral elements.

All vertical sides of the model are fixed in normal direction, while the bottom boundary of the model is fully fixed ('standard' fixities). Sheet pile penetration is modelled by applying prescribed vertical displacements at the top of the pile in steps of 0.05 m, until a maximum penetration depth of 2.5 m is reached. The calculations are performed with the 'standard' MPM formulation as well as with DDMP.

Results

Fig. 3 shows the average vertical stress at the top of the pile as a function of the penetration depth for different soil strengths. The graph shows that the average vertical stress (and hence the total pile bearing capacity) increases with the pile penetration depth. It can be verified that the results of Fig. 3 present a slight over-estimation of the theoretical bearing capacity. This over-estimation can be reduced with mesh refinement and adding more material points to the elements (see also Lim et al. 2013).

Fig. 4 shows the vertical soil stress in a section below the pile, for different pile penetration depths. The vertical location is expressed in the corresponding vertical coordinate (y), where y = 0 represents the bottom of the MPM region. It can be seen that the DDMP calculations give smoother stresses than the pure MPM calculations,

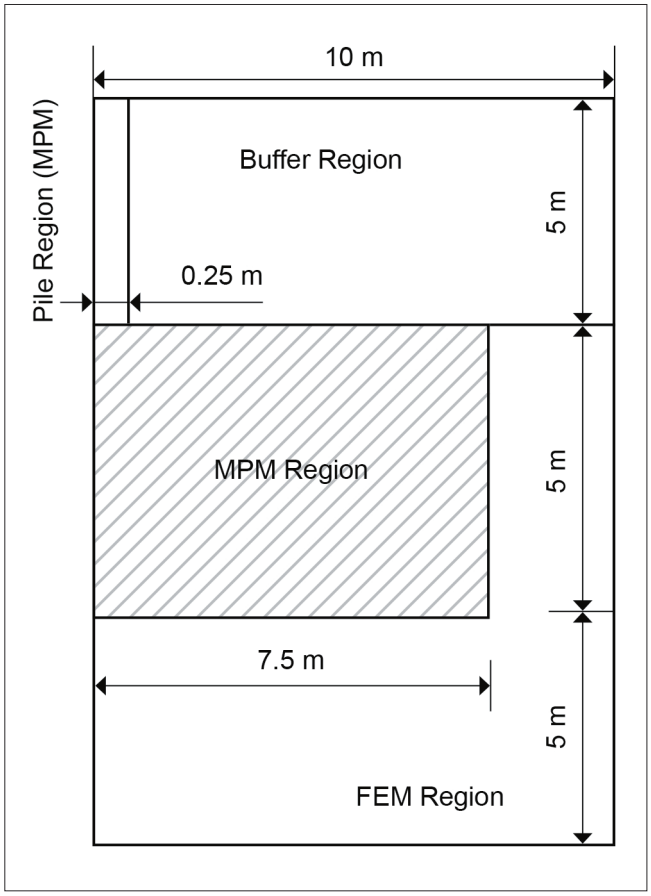

Figure 2: Geometry of pile and soil, with indication of FEM and MPM regions

Bild 2: Pfahl- und Bodengeometrie mit Angabe der FEM- und MPM-Bereiche

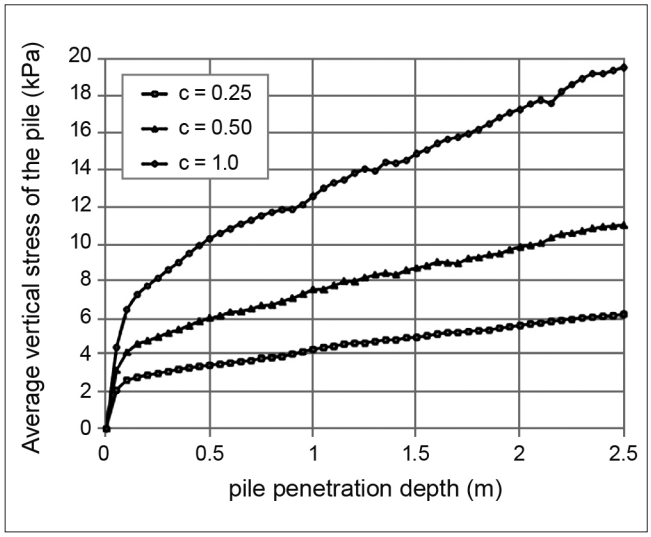

Figure 3: Average vertical stress in the pile as a function of penetration depth (triangular elements)

Bild 3: Durchschnittliche vertikale Spannung im Pfahl in Abhängigkeit von der Eindringtiefe (Dreieckelemente)

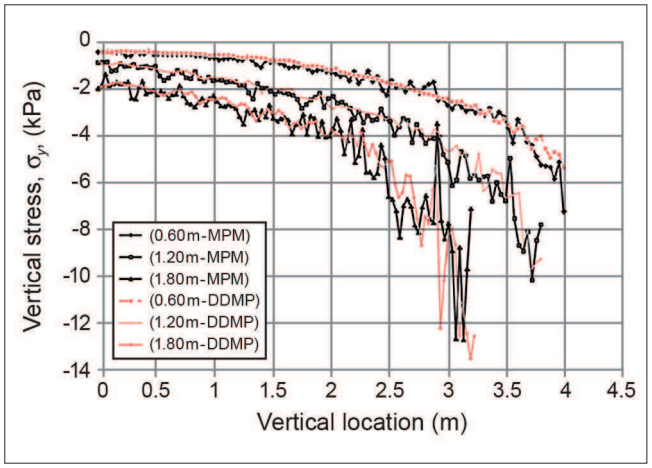

Figure 4: Vertical stress below the pile for different penetration depths (quadrilateral elements)

Bild 4: Vertikale Spannung unterhalb des Pfahls für unterschiedliche Eindringtiefen (Viereckelemente)

although for the deepest penetration none of the results are very smooth.

Based on these results it can be concluded that MPM is usable for pile penetration in cohesive soils, but the accuracy of stresses is limited.

4.2 Spudcan punch through

Durchstanzen einer Spudcan in die Weichschicht

A spudcan is used as a foundation element for offshore platforms in the seabed. Spudcan installation and load testing involves large soil deformation. In situations where there is a stiff soil layer on top of a softer soil layer, the installation of the spudcan may face 'punch-through' failure. This mechanism is caused by a (sudden) decrease of bearing capacity when the spudcan penetrates from the stiff layer into the soft layer. In this application, we have adopted case study 2 of the work presented by Khoa (2013).

On the left of Fig. 5, a 3D slice of the spudcan and the soil medium is shown. Due to axisymmetry of the problem, only $\pi/16$ of the cylinder is taken into account in the 3D model. Standard fixities are applied. Two layers of soil with different soil properties are defined, with layer A indicating a bottom layer of soft clay, while layer B indicates a top layer of stiff clay. For both soil layers, the Tresca model is used as failure criterion, with undrained shear strength of s_{Ua} = 11.0 kN/m² and s_{uB} = 38.3 kN/m² respectively. The soil layers have elastic stiffnesses, E_A = 4933.50 kN/m² and E_B = 17177.60 kN/m², while both layers have an effective Poisson's ratio of ν = 0.333. The self weight of the soil is not taken into account in this simulation and the initial stress state of the soil layers is zero. The undrained condition of the problem is applied by using the (p-u) mixed formulation as mentioned in the Introduction. The spudcan, on the other hand, has dimensions stated on the right of Fig. 5. It is defined as a linear elastic material, with an elastic stiffness about 200 times higher than the elastic stiffness of soil layer B. A smooth contact is applied on the surface of the spudcan.

The computational grid is subdivided into two regions. The first region is the MPM region, which is located near to the area of spudcan penetration. Further away from the penetration area, a FEM region is defined. A buffer zone with height about two elements is defined above the MPM region to capture material points that are moving beyond the original soil surface.

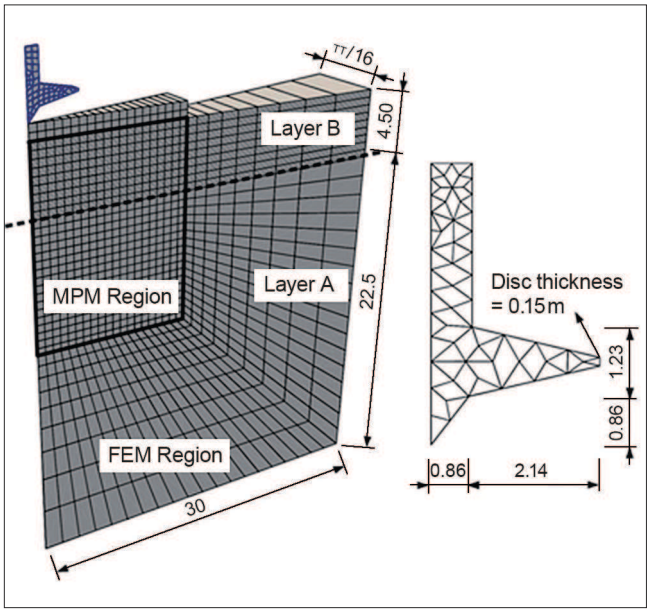

Figure 5: Geometry of the spudcan and soil layers (dimensions in m)

Bild 5: Geometrie von Spudcan und Bodenschichten (Maße in m)

Results

Fig. 6 shows the penetration of the spudcan and the soil deformation at a depth equal to the spudcan diameter. A clear vertical cut is created by the spudcan penetration, but the cut has remained stable during the whole simulation process because the self weight of the soil

layers is not taken into account in this analysis. A plug of stiff soil is trapped below the spudcan, but, in a later stage of penetration, this plug of stiff soil is slowly moving sidewards from the base to the side of the spudcan. This trapped plug of stiff soil was also observed in Case 2 of Khoa (2013).

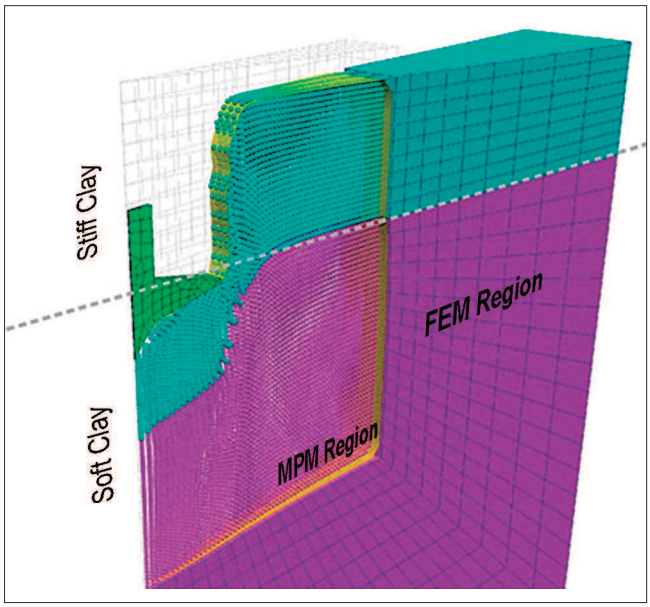

Figure 6: 3D view of the penetration process when the spudcan is at d/D = 1.0
Bild 6: 3D-Darstellung des Eindringvorgangs bei einer Eindringtiefe der Spudcan von d/D = 1,0

Fig. 7 shows the boundary between the FEM and MPM region at the final deformation stage of the spudcan penetration process. By using the mesh relaxation method, we are able to preserve the deformation history of the FEM region, as well as recovering the mesh in the MPM region to the least deformed state.

The bearing response of the soil is presented in Fig. 8. The vertical axis represents the normalized penetration depth of the spudcan, d/D, while the horizontal axis represents the normalized bearing pressure of the soil, $Q_n = q / s_{uB}$. Before the penetration depth of d/D = 0.167, the rate of increment of bearing pressure caused by the penetration of the tip of the spudcan is relatively slow. After d/D = 0.167, the bearing pressure of the soil starts to increase rapidly as more surface of the spudcan is in contact with the soil. The bearing capacity reaches its maximum at about Q_n = 21, which is the point where the surface of the soil is in contact with the full bottom of the spudcan. After the plateau, the bearing capacity of the spudcan started to decrease slowly as the spudcan

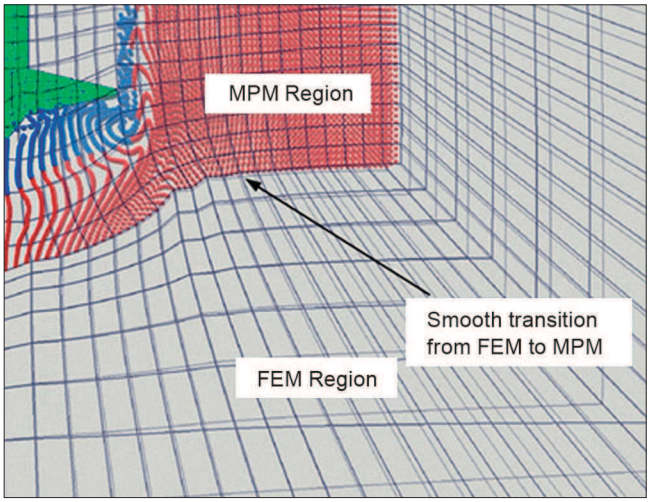

Figure 7: Smooth transition from FEM to MPM
Bild 7: Gleitender Übergang von FEM zu MPM

penetrates further into the soil. This reduction of bearing capacity is caused by the reduction of the effective thickness of the stiff soil layer when the penetration goes deeper into the soil. This phenomenon of reduction in bearing capacity could not be captured by small strain FEM analysis. This punch through failure is significant in spudcan installation processes because the reduction of the bearing capacity in the soil will cause the spudcan to penetrate rapidly into the softer layer. As the spudcan installation is usually performed by placing a weight on top of the spudcan, punch through failure may cause catastrophic loss during the installation of the spudcan.

Based on these results it can be concluded that MPM is usable for spudcan penetration and punch-through in cohesive soils.

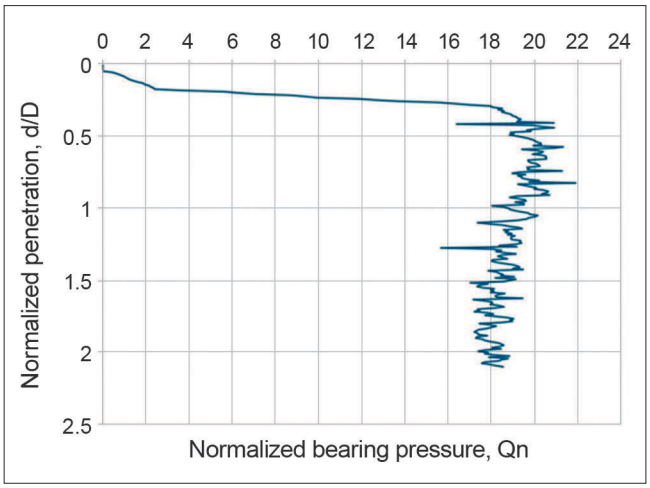

Figure 8: The bearing response of the soil in the spudcan penetration process.
Bild 8: Auflagerreaktion des Bodens beim Eindringen der Spundcan

4.3 Pipeline movement
Bewegung der Pipeline

The third application concerns the movement of a pipeline in the seabed. A pipeline with an outer diameter of 0.8 m is embedded in the seabed and subsequently moved in lateral direction. This movement can have different causes, but the question is which path the pipeline will follow, how the soil is going to be displaced and what is the resistance from the soil.

The soil has an effective (submerged) unit weight of 6.5 kN/m³ and is modelled by means of the linear elastic perfectly plastic Tresca model with an undrained shear strength profile of 2.3 kN/m² at the top and an increase of 3.6 kN/m² per meter depth. The stiffness also increases with depth, following the undrained shear strength profile: $E_s = 500\ s_u$..

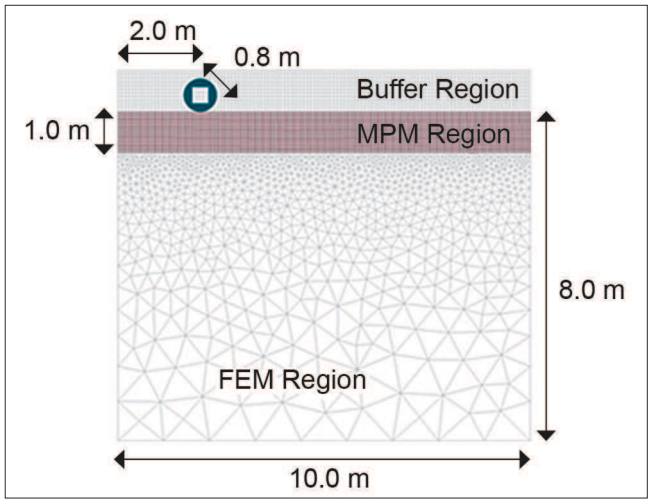

Figure 9: Pipeline model
Bild 9: Modell einer Pipeline

The model used for this situation is a 2D plane strain model (Fig. 9) with an MPM region of 1.0 m thickness consisting of linear quadrilateral elements with 9 material points per element, and a FEM region of 7.0 m thickness consisting of linear triangular elements. Above the ground surface there is a MPM buffer region. The pipeline itself has a weight of 6.0 kN/m and is composed of linear elastic 6-noded triangular finite elements with a stiffness of $E_p = 50\ E_s$. The pipeline is initially 'pushed' into the soil (Phase 1) after which it is 'balanced' at its own weight (Phase 2) before it is moved in horizontal direction at a velocity of 0.24 m/s for more than 2 m by prescribing the horizontal displacement components whilst the vertical components are free (Phase 3). In order to stabilize the calculations (in particular the last phase), the calculations are performed as full dynamic calculations, including inertia and a slight damping of the Newmark-beta scheme as described in 3.8.

Results

Fig. 10 shows the time-settlement curve for the first two phases. It can be seen that there is very little rebound in Phase 2 when the external force is removed.

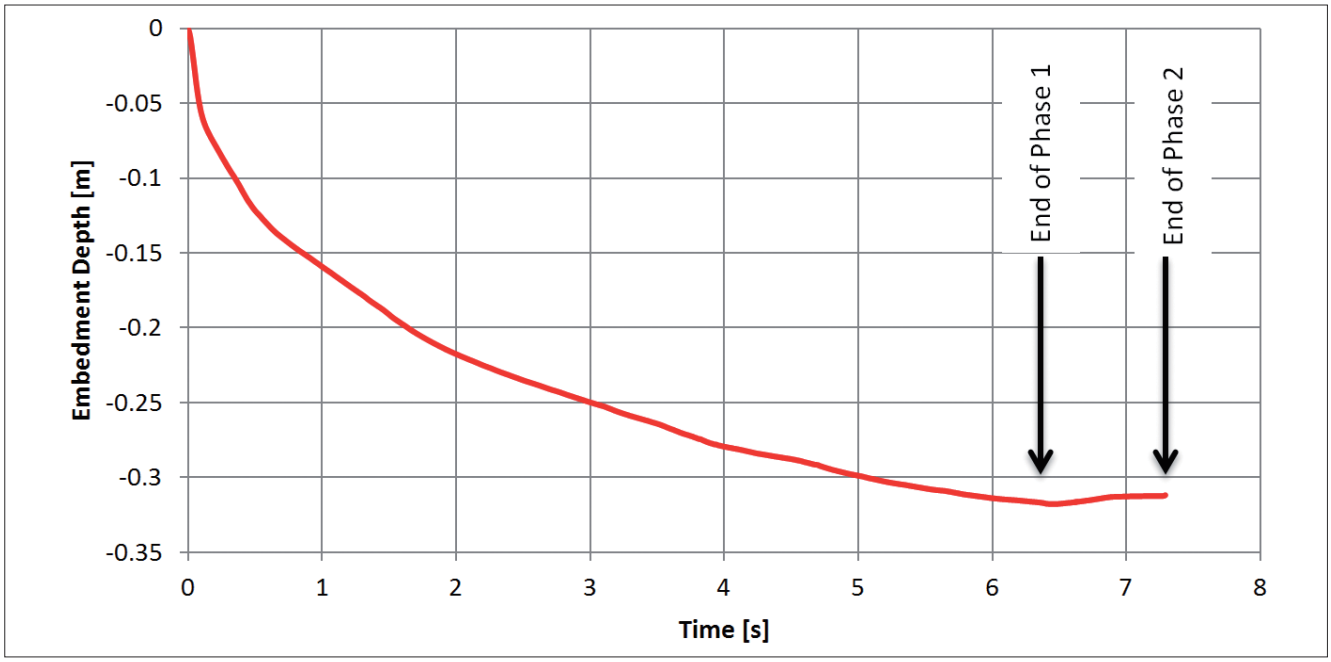

Figure 10: Time-settlement curve of the pipeline during Phase 1 (pushing in) and Phase 2 (balancing)
Bild 10: Zeit-/Setzungskurve der Pipeline während Phase 1 (Einschieben) und Phase 2 (Ausbalancieren)

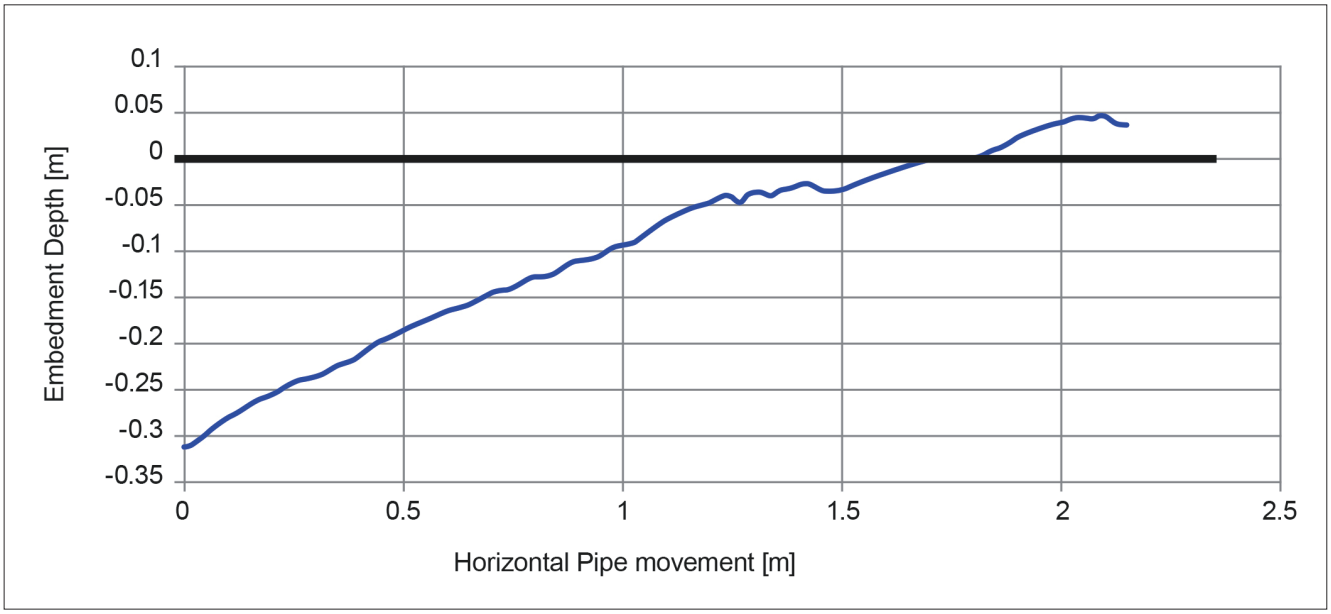

Figure 11: Path of the pipeline in Phase 3 (lateral movement).
Bild 11: Weg der Pipeline in Phase 3 (seitliche Bewegung)

Fig. 11 shows the movement path of the pipeline in Phase 3. The vertical position is obtained from the equilibrium between the self weight of the pipeline and the vertical soil stress, while the pipeline is pushed in lateral direction. Due to the fact that not only the pipeline is pushed, but also the soil in front of the pipeline, a 'heap' of soil is created in front of the pipeline. This 'heap' causes the pipeline to move above the original seabed level, as depicted in Fig. 12.

Noteworthy is the shape of the 'heap' in front of the pipeline, which looks rather unrealistic. It might be expected that the soil should 'fall down' rather than staying in the position as displayed in Fig. 12. Here, the following aspects should be considered:

- Material points do not represent particles, but material volumes with representative properties and state parameters
- The soil has a purely cohesive strength
- It is a dynamic analysis in which inertia effects are taken into account; the end of the analysis is not a steady-state situation
- Elements still have stiffness as long as they contain at least one material point

Based on these results it can be concluded that MPM is usable for pipeline movements in cohesive soils.

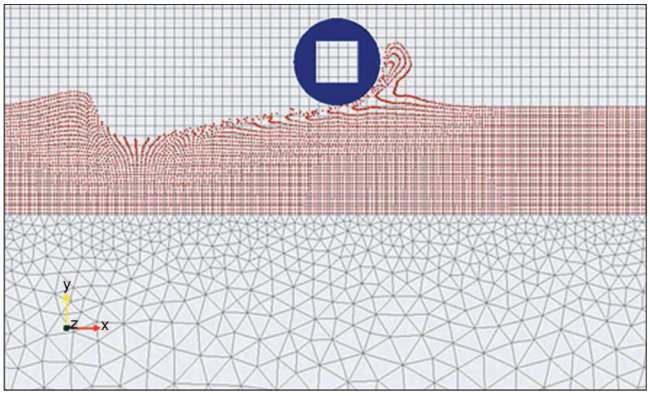

Figure 12: Position of the pipeline at the end of the analysis.
Bild 12: Lage der Pipeline am Ende der Analyse

So far, we have primarily performed analyses for soils in which their strength properties are described by means of undrained shear strength, which is a common approach in offshore geotechnical engineering. The use of effective strength properties (frictional strength) in the Mohr-Coulomb non-associated plasticity model involves some more challenges on numerical stability, which is subject of further research

5 Conclusions
Zusammenfassung

In this contribution some of the challenges have been presented in an attempt to make the material point

method (MPM) for large deformation analysis of soil-structure interaction problems suitable for practical applications. Solutions to these challenges include:

- The use of DDMP to smoothen the stresses and to improve the convergence
- The use of dynamic analysis (inertia and damping) and an automatic time stepping algorithm to make the calculations robust and stable
- A level-set approach to detect model boundaries
- A special level-set contact formulation to model soil-structure interaction

Examples were shown involving offshore geotechnical applications, i.c. the installation of a (sheet) pile, the punch-through of a spudcan and the movement of a pipeline in the seabed. These results cannot be obtained using the 'standard' finite element method. Hence, the material point method offers possibilities to numerically analyse and optimise situations that cannot be modelled with standard FEM. Using the above solutions, we have shown that it is possible to use MPM on a larger scale for offshore geotechnical engineering and design applications.

6 References
Literatur

Andreykiv, A., van Keulen, F., Rixen, D. J. and Valstar, E. (2011): A level-set-based large sliding contact algorithm for easy analysis of implant positioning. International Journal for Numerical Methods in Engineering, Vol. 89, No. 10, pp. 1317-1336.

Bardenhagen, S. G and Kober, E. M. (2004): The generalized interpolation material point method. Computer Modeling in Engineering & Sciences, Vol. 5, No. 6, pp. 477-495.

Belytschko, T., Liu, W. K. and Moran, B. (2000): Nonlinear finite elements for continua and structures. Wiley, Chichester.

Beuth L. (2012): Formulation and application of a quasi-static material point method. PhD Thesis, University of Stuttgart.

Brezzi, F. and Fortin, M. (1991): Mixed and hybride finite element methods. Springer-Verlag, New York.

Glowinski, R., Pan, T.-W., Periaux, J. (1994): A fictitious domain method for Dirichlet problem and applications. Computer Methods in Applied Mechanics and Engineering Vol. 111(3–4), pp. 283–303.

Khoa, H. D. V. (2013): Large deformation finite element analysis of spudcan penetration in layered soils. In: Proceedings of the 3rd International Symposium on Computational Geomechanics (COMGEO III), Krakow, Poland, pp. 570–584.

Lim, L. J., Andreykiv, A. and Brinkgreve, R. B. J. (2013): Pile penetration simulation with material point method. In: M. A. Hicks, J. Dijkstra, M. Lloret-Cabot & M. Karstunen (Eds.) Installation effects in geotechnical engineering – Proceedings of the International Conference on Installation Effects in Geotechnical Engineering, CRC Press, Boca Raton, FL, pp. 24-30.

Lim, L. J., Andreykiv, A. and Brinkgreve, R. B. J. (2014): On the application of the material point method for offshore foundations. In: M. A. Hicks, R. B. J. Brinkgreve & A. Rohe (Eds.) Numerical Methods in Geotechnical Engineering, Taylor & Francis, London, pp. 253-258.

Sulsky, D., Chen, Z. and Schreyer, H. L. (1994): A particle method for history-dependent materials. Computer Methods in Applied Mechanics and Engineering, Vol. 118, pp. 179-196.

Sulsky, D., Zhou, S. J. and Schreyer, H. L. (1995): Application of a particle-in-cell method to solid mechanics. Computer Physics Communications, Vol. 87, pp. 236-252.

Wieckowski, Z. (2004): The material point method in large strain engineering problems. Computer Methods in Applied Mechanics and Engineering, Vol. 193, pp. 4417–4438.

Zhang, D. Z., Ma, X. and Giguere, P. T. (2011): Material point method enhanced by modified gradient of shape function. Journal of Computational Physics, Vol. 230, pp. 6379-6398.